A Changing North Atlantic Background Amplifies Western European Heatwaves

Author Information

Affiliations

Houwen Wang[1], Fanghe Zhao[1,2*], Yuhang Wang[1*], Hsiang-Jui Wang[1], Guanru Wu[3], Shengjun Xi[1], Weichen Liu[2]

[1]School of Earth and Atmospheric Sciences, Georgia Institute of Technology, Atlanta, GA 30332-0340, USA

[2]Department of Atmospheric Science, University of Wyoming, Laramie, WY, 82070, USA

[3]College of Oceanic and Atmospheric Sciences, Ocean University of China, Qingdao, Shandong 266100, China

***Correspondence to:** fzhao@uwyo.edu **;** yuhang.wang@eas.gatech.edu**

Abstract

Western European summer heatwaves have increased markedly since the 1990s, culminating in the record warmth of May–July 2026 since 1950. We show that this rise is closely associated with the slowly evolving North Atlantic background. We combine two leading April sea surface temperature modes, representing basin-wide warming and a tripole-like pattern, into an Atlantic Two-Mode Index (ATMI). The index closely tracks the low-frequency increase in heatwave days and peaked in 2026. Under closely matched heatwave-favoring atmospheric circulation, the post-1990 events were 1.3 °C warmer than historical counterparts despite little change in atmospheric ridge amplitude; removing the ATMI-linked low-frequency temperature component reduced this difference to 0.1 °C. Persistent heatwaves occurred in 90% of cases under high-ATMI conditions but were absent under low-ATMI conditions. These results

indicate that western European heatwaves have become more frequent mainly because a warmer Atlantic–European background allows similar circulation patterns to produce substantially greater heat extremes.

Introduction

Western Europe is a hotspot of rapidly increasing heatwave activity. The exceptional events of 2003, 2010, 2018, 2019 and 2022 demonstrated that persistent circulation anomalies, land–atmosphere feedbacks and a warmer baseline can combine to produce temperatures outside historical experience [1, 2, 3, 4, 5, 6, 7, 8]. The key question is therefore how circulation organizes heatwaves in space and time, and how the evolving background climate alters the thermal outcome of that circulation.

Separating these influences is particularly important in western Europe, where summer heat extremes have increased faster than in many climate-model simulations. Recent studies attribute this excess warming to a combination of an unusually large circulation contribution, regional thermodynamic amplification associated with aerosol decline and surface brightening, and forced changes in variability and land–atmosphere coupling [9, 10, 11, 12, 13]. Blocking, persistent jet configurations and recurrent planetary-wave patterns are important features of individual heatwaves, but their long-term trends and responses to forcing remain uncertain and region dependent. [14, 15, 16, 17, 18, 19]. Understanding the escalation of western European heatwaves therefore requires determining whether comparable heat-favoring circulation produces different thermal outcomes as the background climate evolves.

The North Atlantic is a plausible source of such slowly varying background variability. Its sea surface temperature (SST) anomalies persist longer than synoptic weather, while basin-scale warmth and meridional SST gradients have been linked to European summer circulation [20, 21, 22, 23, 24]. Spring North Atlantic SST patterns have also been associated with subsequent European summer circulation and heatwaves, including through non-overlapping precursor windows and model-based experiments [25, 26, 27, 28]. Yet whether this antecedent Atlantic state is linked to the recent rise in western European heatwaves, and whether the stronger heat produced under comparable circulation is specifically associated with its slowly evolving background, remain unresolved. We therefore focus on April, the latest fully antecedent month before the May–July target season and investigate whether this pre-season Atlantic state distinguishes subsequent heatwave susceptibility under comparable atmospheric circulation.

Here we examine how the rise in western European heatwave activity since the 1990s relates to a slowly varying North Atlantic background across 1950–2026, with the record 2026 season representing its most extreme manifestation. We identify two leading April SST modes whose regression-weighted combination defines an Atlantic Two-Mode Index (ATMI) whose low-frequency evolution closely tracks May–July heatwave activity. The ATMI reached a record high in April 2026, while high-ATMI conditions are associated with stronger upward latent heat flux and a vertically aligned Atlantic trough–European ridge pattern. Crucially, comparable heat-favoring atmospheric circulation produces markedly different thermal outcomes across ATMI states, with persistent heatwaves strongly concentrated under high-ATMI conditions. Together, these results show that the recent rise in western European heatwaves, and its extreme expression in 2026, tracks the low-frequency evolution of the North Atlantic background rather than a change in the event-scale circulation that produces individual heatwaves.

Results

Record western European heatwave season in 2026

The May–July 2026 heatwave season was the warmest on record in western Europe during 1950–2026 (Fig. 1). The preceding April SST field exhibited a pronounced warm–cool–warm structure across the North Atlantic, while the subsequent May–July circulation featured a corresponding central Atlantic trough–western European ridge pattern (Fig. 1b). The strongest surface warming extended across much of western and central Europe and coincided with positive geopotential height (Z500) anomalies extending from the eastern North Atlantic into the continent (Fig. 1a,b). ERA5 daily maximum temperature (Tmax) averaged over the western European domain (10° W–20° E, 40–55° N) was 3.2 °C above the 1981–2010 calendar-day climatology (Fig. 1a), while the corresponding regional Z500 anomaly was 56 m (Fig. 1b). Using a regionalized version of the CTX90 framework, which identifies extreme heat based on exceedance of the local calendar-day 90th percentile of daily Tmax, we defined a heatwave day as one on which at least one-third (33.3%) of western European land area exceeded this threshold. A heatwave event was defined as at least three consecutive heatwave days. May–July 2026 contained 45 heatwave days, 43 of which occurred within four heatwave events. The two strongest events occurred in late May and late June, when regional Tmax anomalies reached 8.7 °C and 9.4 °C, respectively, while 95.2% and 92.2% of western European land area exceeded their local thresholds.

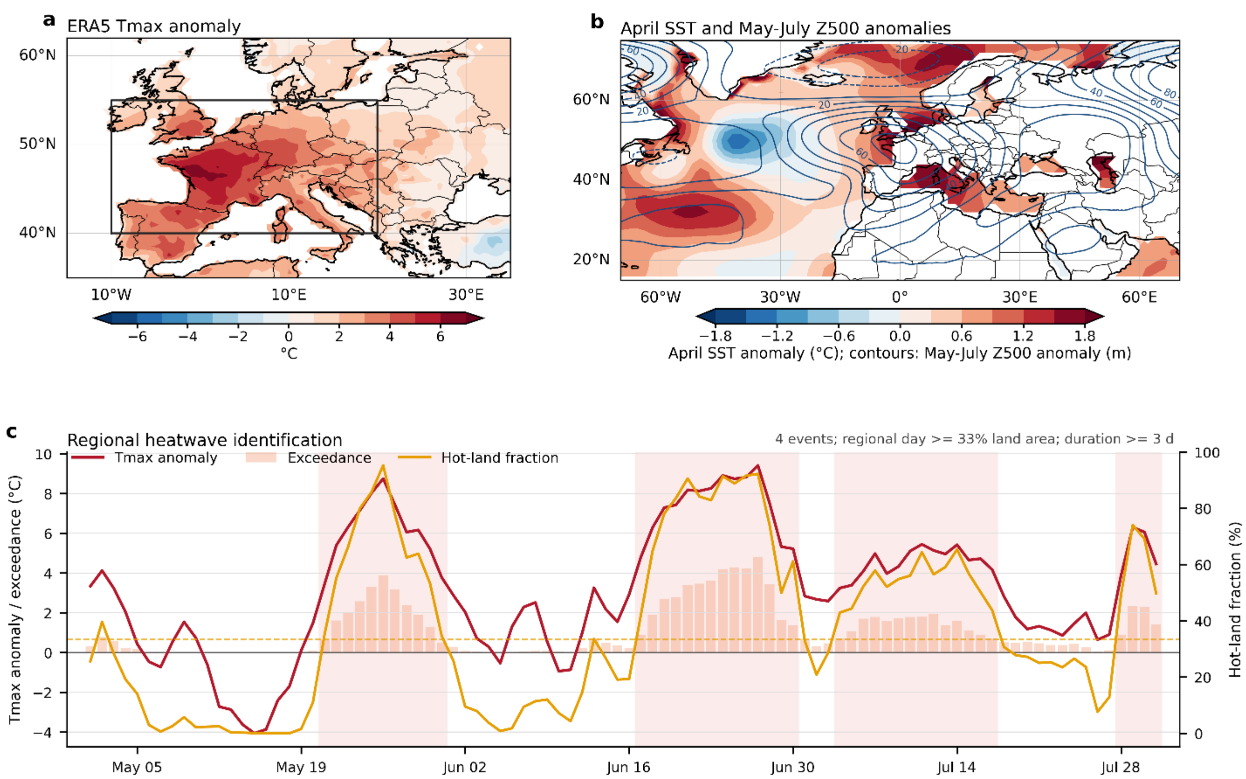

Fig. 1. Record western European heatwave season during May–July 2026. a, b, Mean ERA5 anomalies for 1 May–31 July 2026 relative to the 1981–2010 climatology: **a,** daily maximum temperature (Tmax; °C), with the western European domain (10° W–20° E, 40–55° N) outlined; **b,** April 2026

ERSSTv5 SST anomaly (shading; °C) and May–July 2026 ERA5 500-hPa geopotential-height anomaly (Z500; contours; m). **c,** Regional Tmax anomaly (red line), regional mean positive exceedance above the local calendar-day 90th-percentile Tmax threshold (bars; °C), and fraction of western European land area exceeding that threshold (orange line). The orange line denotes the one-third land-area criterion for a regional heatwave day; pink shading marks four events satisfying this criterion for at least three consecutive days.

The temporal evolution further shows that the exceptional seasonal warmth was organized into distinct heatwave events rather than a single persistent event (Fig. 1c). During the major peaks, higher regional Tmax coincided with greater exceedance above local heat thresholds and a rapid expansion of the land area exceeding those thresholds. The late-May, late-June, mid-July and late-July events were separated by cooler intervals, consistent with recurrent synoptic heat episodes superimposed on a persistently warm thermal background.

The record seasonal warmth and recurrent heatwave events motivate separating the synoptic circulation organizing individual heatwaves from the slower thermal background in which they developed. The pronounced April Atlantic SST anomalies preceding the 2026 season therefore raise the question of whether a comparable Atlantic state has accompanied western European heatwave activity across the full record, and in particular its rise since the 1990s.

A North Atlantic SST pattern tracks western European heatwave activity

April North Atlantic SST exhibits a coherent basin-scale pattern associated with subsequent western European May–July temperature (Fig. 2a). Positive correlations extend across much of the subtropical and eastern North Atlantic, with an opposing signal over the subpolar basin. The broad SST contrast evident in April 2026 (Fig. 1b) is also recovered in the full-record SST–temperature relationship (Fig. 2a). To obtain a compact representation of this SST structure, we applied EOF analysis to April SST anomalies over the North Atlantic (80° W–0°, 10–70° N; Methods). EOF1 captures a basin-wide warm structure resembling Atlantic Multidecadal Variability (AMV) and explains 35.3% of the variance in standardized April North Atlantic SST anomalies. EOF2 explains a further 18.5% and resembles a tripole-like North Atlantic SST pattern, emphasizing the contrast between subtropical and subpolar anomalies (Fig. 2b,d). Together, the two modes explain 53.8% of the variance in the standardized April North Atlantic SST field. Basin-scale North Atlantic variability has long been linked to multidecadal changes in European summer climate and heatwave occurrence[20, 21, 29], whereas tripolar SST structure is a characteristic of coupled North Atlantic atmosphere–ocean variability [30]. The two modes therefore provide complementary representations of the basin-wide and meridional SST structures associated with subsequent western European warmth.

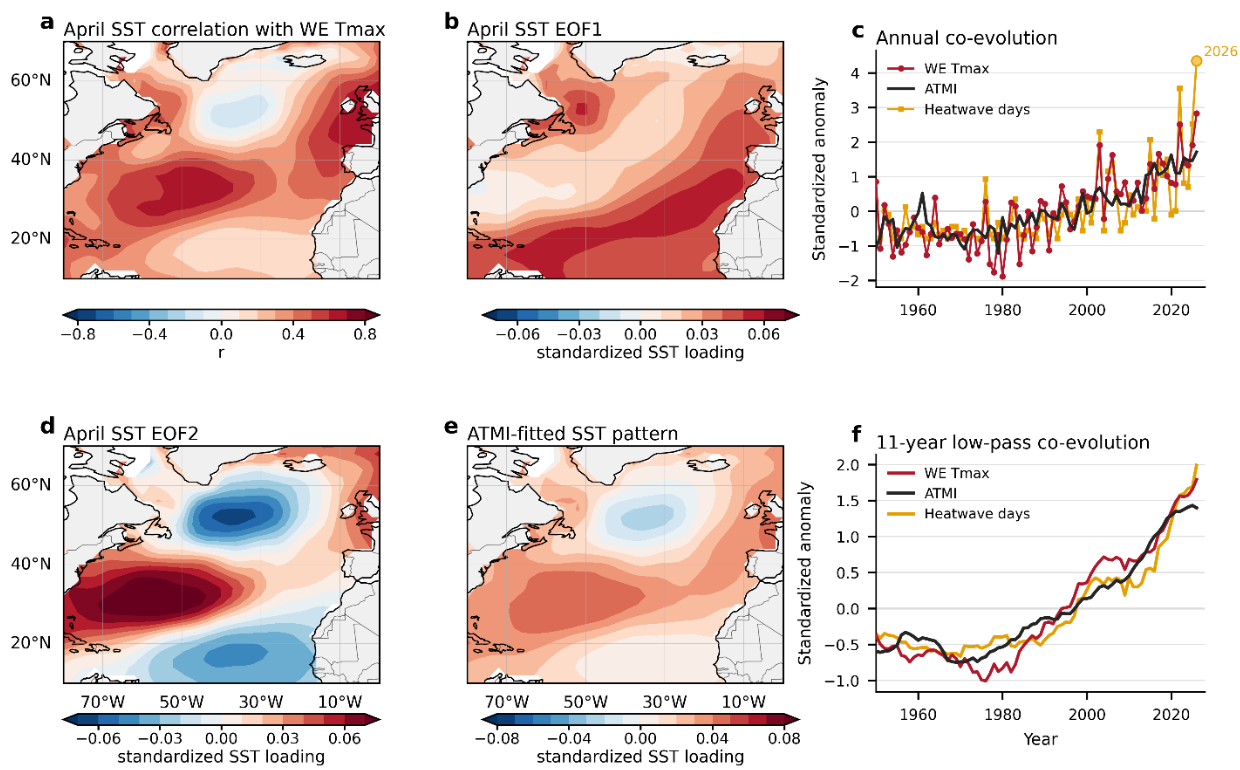

Fig. 2. April North Atlantic SST modes associated with subsequent western European May–July temperature and heatwave activity. a, Correlation between April SST and western European (WE) May–July maximum temperature (Tmax) during 1950–2026. **b,d,** Leading two correlation empirical orthogonal functions (EOFs) of April North Atlantic SST. **c,** Standardized annual WE May–July Tmax,

the corresponding April Atlantic Two-Mode Index (ATMI), and heatwave-day frequency, with 2026 highlighted. **e,** ATMI-associated SST pattern, obtained from the regression-weighted combination of EOF1 and EOF2, which closely reproduces the direct SST–temperature correlation pattern in panel a (spatial r = 0.93). **f,** 11-year running means of WE May–July Tmax, the ATMI and heatwave-day frequency. In c, red, black, and orange lines show annual standardized WE Tmax, ATMI, and heatwave-day frequency, respectively; in f, the corresponding thick curves show their 11-year running means.

To combine the two leading April SST modes, we regressed standardized western European May–July Tmax simultaneously onto the two standardized principal components during 1950–2026. The resulting weighted combination defines the Atlantic Two-Mode Index (ATMI). Applying the same regression weights to EOF1 and EOF2 yields the ATMI-associated SST pattern (Fig. 2e). This pattern closely reproduces the direct April SST May–July Tmax correlation pattern (Fig. 2a), with a spatial pattern correlation of 0.93 across common ocean grid points within the North Atlantic EOF domain. Previous studies identified spring North Atlantic SST precursors using prescribed SST dipoles linked to later Euro-Atlantic circulation[26] or spatially distributed regional SST features extracted from large-ensemble simulations[27]. Here, the two leading April SST modes recover most of the observed SST–temperature pattern without prescribing regional SST centers or combining multiple regional predictors. The ATMI therefore provides a parsimonious representation of the Atlantic state, with which we characterize the slowly varying background against which heat-favoring circulation is realized.

The two-mode regression accounts for 54.1% of the raw annual variance in western European May–July temperature (r = 0.74) during 1950–2026 (Fig. 2c). After separating linear detrending, the corresponding association weakens to r = 0.37, equivalent to 13.4% of the variance, indicating that much of the association resides in shared low-frequency evolution. Although heatwave occurrence is not used to construct the ATMI, annual heatwave-day frequency also covaries strongly with the index (r = 0.64, $P < 0.001$; Fig. 2c). This relationship becomes particularly pronounced at low frequencies. The 11-year low-frequency ATMI correlates with Tmax at r = 0.97 and with heatwave-day frequency at r = 0.96 (Fig. 2f).

Thus, the Atlantic state tracks not only the gradual warming of May–July conditions but also the increasing frequency with which temperatures cross the heatwave threshold. The dominance of the low-frequency component is consistent with previous evidence that North Atlantic multidecadal variability can modulate European summer climate and heatwave occurrence[20, 21, 29]. We therefore interpret the ATMI as a compact index of the slowly evolving thermal background of western Europe. Because April precedes May–July, the SST signal provides a temporally distinct precursor to the subsequent heatwave season. Consistent with previous evidence of coupled North Atlantic SST–circulation evolution[28], the strong low-frequency correspondence supports a directional influence of the Atlantic state on subsequent European summer conditions.

April 2026 represented the most extreme positive expression of this historical relationship. The pronounced warm–cool–warm SST structure evident that April (Fig. 1b) corresponded to an ATMI of 1.7 standardized units, the highest value in the 77-year record (Fig. 2c). May–July 2026 subsequently recorded 45 heatwave days, also the highest value in the 1950–2026 record. The fitted May–July temperature anomaly was 1.7 °C, compared with the observed 3.2 °C on the same regression baseline. Thus, 2026 sat at the warm end of the slowly evolving background, but that background accounts for only about half of the realized heat. This motivates examining how the background has changed over the record and how it combines with heat-favoring circulation.

North Atlantic warming pattern tracks the rise in western European heatwaves since 1990

Years in the upper quartile of the annual ATMI differ markedly from lower-quartile years. The composite difference shows the characteristic warm–cool–warm Atlantic SST structure together with a coherent May–July Z500 wave train, comprising positive height anomalies over the western North Atlantic, a central Atlantic trough and downstream ridging across western and northern Europe (Fig. 3a;

20 years per group). A similar broad configuration is evident in 2026 (Fig. 1b), consistent with the ATMI capturing a slowly varying Atlantic state linked to downstream European circulation.

The associated surface heat exchange is consistent with a thermodynamic pathway from the Atlantic SST state to the overlying atmosphere (Fig. 3b). High-ATMI conditions feature stronger upward latent heat flux over substantial parts of the North Atlantic, indicating enhanced ocean-to-atmosphere latent heat transfer. The corresponding Z850 anomalies closely resemble the Z500 wave train, with a central Atlantic trough and downstream European ridge vertically aligned through the lower and middle troposphere. This near-barotropic structure supports a coherent downstream circulation configuration favorable for European heatwaves. Positive height anomalies over western Europe promote subsidence, reduced cloudiness and weak ventilation, while ridge position further regulates warm-air advection and radiative heating[9, 14, 18]. The April SST state, the May–July upward heat-flux anomalies and the vertically aligned circulation anomalies are therefore physically consistent with a North Atlantic contribution to western European heatwaves, although a same-season composite cannot establish that the ocean drives the ridge rather than responding to it.

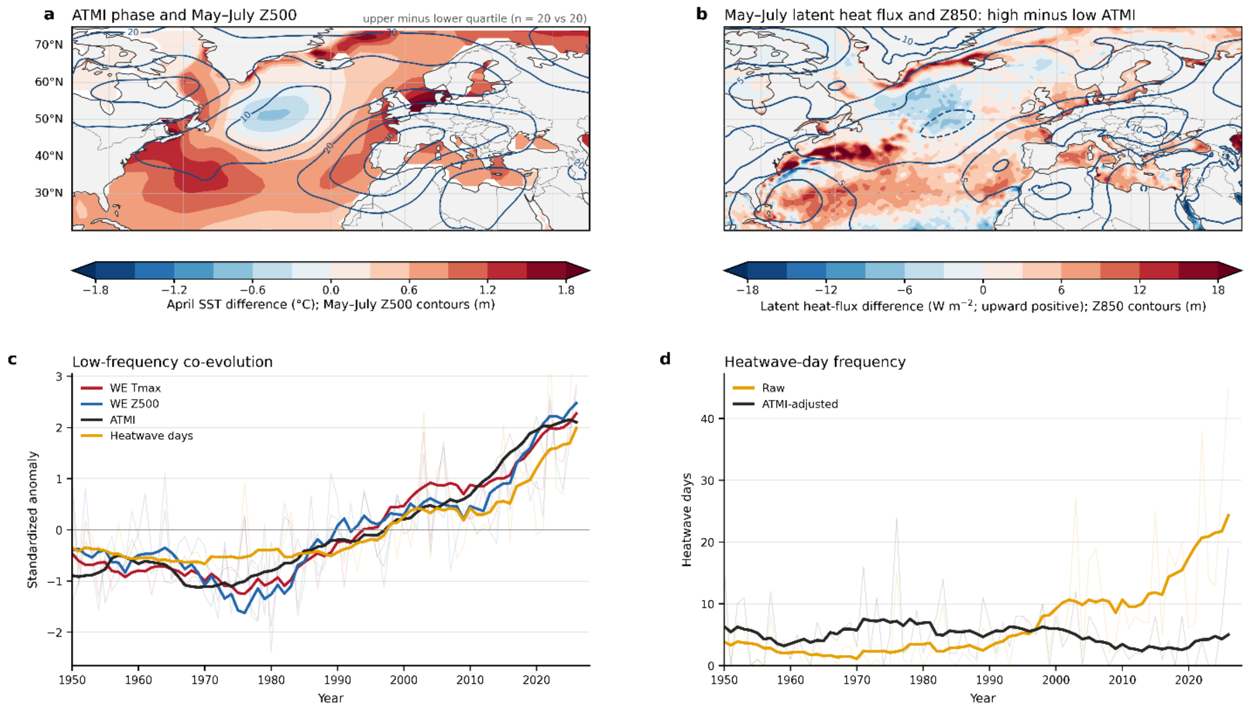

Fig. 3. Atlantic background, circulation and western European heatwave occurrence. a, Composite difference between years in the upper and lower quartiles of the annual ATMI (20 years per group). Shading shows the April SST difference (°C), and contours show the corresponding May–July Z500 difference (m). **b,** May–July latent heat-flux difference between upper- and lower-ATMI years (shading; W m^{-2}; positive upward), with the corresponding Z850 difference shown by contours (m). **c,** Annual and 11-year standardized anomalies of the ATMI, western European (WE) Tmax, WE Z500 and heatwave-day frequency during 1950–2026. Black, red, blue, and orange curves denote ATMI, WE Tmax, WE Z500, and heatwave-day frequency, respectively. WE Tmax and Z500 are averaged over 10° W–20° E, 40–55° N; faint lines denote annual values and thick lines the 11-year running means. **d,** Annual heatwave-day frequency before and after removal of the low-frequency temperature component statistically associated with the ATMI; orange and black curves denote the raw and ATMI-adjusted series, respectively, and thick lines show the corresponding 11-year series.

This background has changed markedly over time (Fig. 3c). The 11-year running means of the ATMI, western European May–July Tmax, western European Z500 and heatwave-day frequency show a coherent low-frequency evolution, with relatively low values before the 1990s followed by a pronounced and sustained increase thereafter. The ATMI is strongly correlated with western European Z500 at this timescale (r = 0.95), while low-frequency Z500 similarly covaries with heatwave-day frequency (r = 0.94). The recent strengthening of the North Atlantic warming pattern therefore coincides with both enhanced European ridging and the sharp increase in heatwave occurrence.

This slowly evolving background does not replace the role of shorter-term atmospheric circulation. Western European May–July Tmax and Z500 remain strongly correlated at the annual scale (r = 0.91), and this relationship persists after their separately fitted ATMI-linked low-frequency components are removed (r = 0.86). The results distinguish two superimposed influences: a slowly evolving Atlantic-linked background that modulates thermal susceptibility, and shorter-term circulation variability that governs when that susceptibility is realized as extreme heat.

Western European heatwave-day frequency rises sharply from the 1990s onward (Fig. 3d), but this increase is largely removed after subtracting the low-frequency temperature component statistically associated with the ATMI. Thus, much of the recent increase in heatwave days shares the slow thermal evolution captured by the North Atlantic warming pattern. This interpretation is consistent with recent decompositions of European warming in which circulation largely determines the timing and geography of individual events, whereas greenhouse-gas warming, aerosol decline, surface brightening and land feedbacks alter the temperature realized under a given flow [9, 10, 11]. We therefore next hold circulation approximately fixed and test whether the warmer background makes comparable heat-favoring flow more likely to produce a heatwave.

Similar atmospheric circulation produces more heatwaves under a warmer Atlantic background

We use flow analogues to test whether similar heatwave-favoring atmospheric circulation produces different thermal outcomes under different background states [32, 33, 34]. A fixed heatwave-reference circulation is constructed from daily eddy-Z500 anomalies within ±2 days of all identified regional heatwave-event peaks during 1950–2026, comprising 318 unique May–July event-window days from 65 events. All May–July days are ranked by their similarity to this pattern over the Atlantic–European domain (50° W–70° E, 25–75° N; Fig. 4a; Methods). The reference circulation resembles a blocking-like Omega configuration, with a strong western European ridge embedded within a broader Atlantic–European wave pattern[35]. Temperature is not used in analogue selection. The primary comparison uses the 100 closest days selected separately from the historical period (1950–1990) and the recent period (1991–2026), corresponding to the periods before and after the pronounced low-frequency increase evident from the 1990s onward (Fig. 3c).

The reference pattern captures atmospheric circulation associated with a substantial fraction of observed heatwave-event peaks (Fig. 4b). At least one top-100 analogue occurs within ±2 days of the peak for 31% of recent events above the median peak intensity (Methods), 46% of those above the 75th percentile and 50% of those above the 90th percentile. The increasing representation toward more intense events indicates that the selected analogues preferentially capture circulation associated with the stronger observed heatwaves.

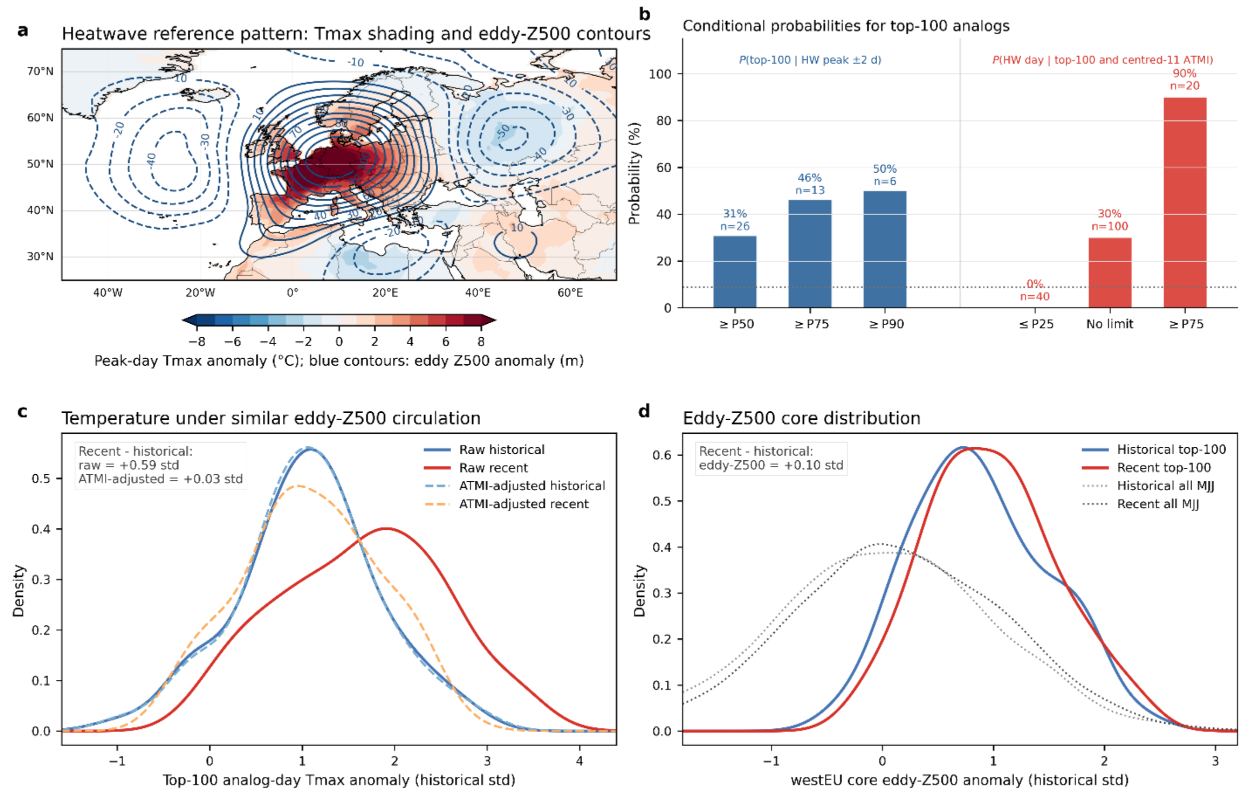

Fig. 4. Heatwave probability and temperature under similar eddy-Z500 circulation. a, Full-record heatwave-reference Tmax anomaly (shading; °C) and eddy-Z500 anomaly (contours; m). Analogue ranking is based only on eddy-Z500. **b,** Conditional probabilities for recent (1991–2026) top-100 analogues. Blue bars show the percentage of heatwave events above each peak-intensity threshold that include a top-100 analogue within ±2 days of the event peak. Red bars show the percentage of top-100 analogue days that fall within an identified heatwave event, overall and under lower- and upper-quartile low-frequency ATMI conditions. Low-frequency ATMI quartiles were defined over 1991–2026. **c,** Kernel-density distributions of standardized Tmax for historical (1950–1990) and recent (1991–2026) top-100 analogue days before and after removing the low-frequency temperature component statistically associated with the ATMI. **d,** Corresponding kernel-density distributions of the standardized western European eddy-Z500 core.

Despite closely matched atmospheric circulation, its thermal impact has changed markedly. Recent top-100 analogues are 1.3 °C warmer than their historical counterparts (95% bootstrap interval, 0.5–2.1 °C; Fig. 4c). To assess whether this difference simply reflects stronger event-scale ridging, we define the eddy-Z500 core as the mean eddy-Z500 anomaly over western Europe (10° W–20° E, 40–55° N). The core differs by only 6 m between recent and historical analogues (95% bootstrap interval, −10 to 19 m; Fig. 4d). Thus, within closely matched heatwave-favoring circulation, the recent warming is not accompanied by a comparable increase in event-scale eddy-Z500 ridge amplitude. Previous flow-analogue studies have established that comparable circulation can yield stronger heat in a warmer climate[33, 34]. Here, we test whether this matched-flow warming is associated with the slowly evolving Atlantic background captured by the ATMI.

Removing the low-frequency temperature component statistically associated with the ATMI reduces the recent-minus-historical contrast from 1.3 °C to 0.1 °C (95% bootstrap interval, −0.6 to 0.7 °C). The matched-flow warming therefore largely disappears after removal of the ATMI-linked background, indicating that the excess heat under similar circulation shares the low-frequency thermal evolution captured by the Atlantic state. A complementary analysis provides consistent evidence without any temperature adjustment (Fig. 4b). Among recent top-100 analogues, none of the 40 days under lower-quartile low-frequency ATMI conditions occurred within a heatwave event (0/40; seven years), whereas 18 of 20 days under upper-quartile conditions did (18/20; 90%; five years). The year-clustered 95% interval for the upper-quartile probability is 76.5–100%. Because the low-frequency ATMI increases through the recent period, lower-quartile years are concentrated early and upper-quartile years late within 1991–2026, so this contrast partly measures the change across the recent period itself. Thus, even under closely similar heatwave-favoring circulation, whether that circulation occurs within a persistent heatwave depends strongly on the background state indexed by ATMI. This state dependence is consistent with modeling evidence that Atlantic multidecadal SST variability modulates Euro-Mediterranean heatwaves[29], but extends that result by conditioning directly on closely matched circulation. Together, the temperature-adjustment and conditional-probability analyses show that the thermal impact of comparable heat-favoring circulation, and its likelihood of occurring within a persistent western European heatwave, have risen together with the slowly evolving Atlantic background.

Discussion

Our results show that the recent rise in western European heatwaves cannot be explained by event-scale atmospheric circulation variability alone. The slowly evolving North Atlantic SST background captured by the ATMI closely tracks the increase in heatwave occurrence since the 1990s and reached its strongest state in April 2026, preceding the exceptional 2026 heatwave season. Under closely matched heatwave-favoring circulation, recent top-100 analogues were 1.3 °C warmer than historical counterparts despite little change in event-scale eddy-Z500 ridge amplitude, and removing the ATMI-linked low-frequency temperature component reduced this contrast to 0.1 °C. Likewise, none of the 40 analogues under lower-quartile low-frequency ATMI conditions occurred within a heatwave event, compared with 18 of 20 (90%) under upper-quartile conditions. These results show that similar heat-favoring atmospheric circulation can produce markedly different heatwave outcomes depending on the background state.

These findings support a background-conditioned framework for western European heatwaves. The North Atlantic SST state should be interpreted here as part of a coupled climate background rather than as a purely one-way atmospheric forcing, consistent with recent evidence that two-way atmosphere–ocean coupling contributed to the extreme North Atlantic SST state in 2023 [36, 37]. In our analysis, high-ATMI conditions are associated with stronger upward North Atlantic latent heat flux and a vertically aligned Atlantic trough–European ridge pattern, a configuration that is physically consistent with an Atlantic contribution to European heatwave susceptibility. The slowly varying background modulates the thermal impact of atmospheric circulation, whereas shorter-term circulation determines when and where that susceptibility is realized. The low-frequency evolution of this background may include contributions from both external forcing and internally generated variability[31], and our observational analysis does not uniquely isolate their respective roles.The temporal lead of the April SST state, together with the associated surface heat-flux and vertically coherent circulation anomalies, supports an antecedent Atlantic contribution to this evolving heatwave susceptibility, although the observational analysis does not uniquely isolate the SST-forced component from broader coupled variability.

The broader implication is that increasing heatwave risk need not require an equivalent strengthening of heat-favoring atmospheric circulation. Across 1950–2026, event-scale atmospheric ridge amplitude under matched flow changed little, whereas the temperature realized under that the atmospheric circulation pattern rose with the background, and the frequency of heatwave days rose with it. The ATMI provides a compact description of where that background change is expressed in the North Atlantic. Because it uses only April SST, it also offers a pre-season measure of the background state, although any seasonal-forecast use would require cross-validated skill against benchmarks based on global mean temperature, basin-mean Atlantic SST and persistence, and targeted SST-pacemaker experiments would be needed to isolate the contribution of the Atlantic SST pattern itself. As the Atlantic background continues to evolve, similar atmospheric flow can be expected to produce progressively more severe thermal outcomes.

Methods

Heatwave definition

Daily Tmax, latent heat flux, Z850 and Z500 for 1950–2026 were obtained from ERA5 [38], and monthly SST from NOAA ERSSTv5[39]. ERA5 latent heat flux was converted to an upward-positive convention. Heatwaves were identified using a regionalized CTX90 framework[13, 40, 41, 42]. At each land grid cell, the threshold was the calendar-day 90th percentile of Tmax during 1981–2010, calculated using a centered 15-day window. Following regional European heatwave studies that impose a minimum spatial-extent criterion to identify spatially coherent events[43, 44], a heatwave day was defined as a day on which at least one-third (33.3%) of the land area within the western European domain (10° W–20° E, 40–55° N) exceeded its local threshold, and a heatwave event as at least three consecutive heatwave days.

Heatwave-day frequency refers to the number of heatwave days within each May–July season. This metric includes isolated heatwave days that do not form a three-day event. Event membership in Fig. 4 refers only to days within identified heatwave events lasting at least three consecutive days. For the event-based analysis in Fig. 4, heatwave intensity was defined as the maximum western European land-mean Tmax anomaly attained during each event, and the corresponding day was defined as the event peak. Peak-intensity percentiles used in Fig. 4b were calculated from the 1991–2026 heatwave-event distribution.

April Atlantic state and circulation

April ERSSTv5 SST anomalies were first calculated relative to the 1981–2010 climatology over the North Atlantic (80° W–0°, 10–70° N). To construct correlation EOFs, the 1950–2026 April anomaly series at each grid cell was subsequently recentered by its full-period mean, divided by its full-period standard deviation, and multiplied by the square root of cosine latitude before singular-value decomposition[45, 46]. The resulting correlation EOFs were oriented such that positive principal components were associated with warmer western European May–July conditions. Standardized western European May–July Tmax was regressed simultaneously onto standardized PC1 and PC2 over 1950–2026. The regression-weighted combination defines the Atlantic Two-Mode Index:

$$\mathrm{ATMI}(t) = \beta_1\,\mathrm{PC}_1(t) + \beta_2\,\mathrm{PC}_2(t).$$

Following common practice for isolating decadal variability in the North Atlantic, low-frequency variability was represented by centered 11-year running means [47, 48], with incomplete endpoint windows retained when at least six years were available. The effective window therefore decreases from 11 years to six years toward the record endpoints, without interpolation or extrapolation. Western European May–July Tmax and Z500, each averaged over 10° W–20° E, 40–55° N, were separately regressed onto the corresponding low-frequency ATMI. For adjusted heatwave detection, the ATMI-linked low-frequency temperature component (°C) was subtracted uniformly from daily Tmax at every land grid cell. The original 1981–2010 local thresholds were retained, and heatwave days and events were reidentified using the same one-third land-area and three-day criteria. The same year-specific low-frequency temperature offset was subtracted from regional daily Tmax in the flow-analogue analysis.

Flow-analogue analysis

Flow analogues were used to compare temperatures under closely matched circulation[32, 33, 34, 49]. Daily eddy-Z500 was calculated by first removing the daily zonal-mean Z500 and then subtracting the 1981–2010 calendar-day climatology of the resulting eddy field. The reference circulation was the mean eddy-Z500 anomaly within ±2 days of all CTX90 heatwave-event peaks during 1950–2026, using 65 events and 318 unique May–July event-window days.

All May–July days during 1950–2026 were ranked by their cosine-latitude-weighted root-mean-square distance from this reference over the Atlantic–European analogue domain (50° W–70° E, 25–75° N). For each day, the analogue distance was calculated as

$$D(t) = \left[\frac{\sum_i w_i \left\{Z'_i(t) - Z'_{i,\mathrm{ref}}\right\}^2}{\sum_i w_i}\right]^{1/2}, \qquad w_i = \cos(\phi_i).$$

where $Z'_i(t)$ is the daily eddy-Z500 anomaly at grid cell i, $Z'_{i,\mathrm{ref}}$ is the full-record heatwave-reference eddy-Z500 anomaly, and $w_i = \cos(\phi_i)$, with ϕ_i denoting latitude. For consistency with the pronounced low-frequency rise evident from the 1990s onward (Fig. 3c), we define 1950–1990 as the historical period and 1991–2026 as the recent period. The analysis then selected the 100 May–July days with the smallest distance separately within the two periods. For Fig. 4c,d, Tmax and eddy-Z500 values were standardized by the mean and standard deviation of all historical May–July days. Distributions were visualized using Gaussian kernel-density estimates with Scott's default bandwidth[50]. These density curves were used only for display, whereas uncertainty in analogue contrasts was estimated by the clustered bootstrap. Event-scale ridge amplitude was quantified as the regional mean eddy-Z500 over western Europe (10° W–20° E, 40–55° N), hereafter referred to as the western European eddy-Z500 core.

Statistical analysis

Analogue uncertainty was estimated using 2,000 year-clustered bootstrap replicates. Within the historical and recent periods separately, years were resampled with replacement, and all selected analogue days from each sampled year were retained together. This preserves within-summer dependence among analogue days rather than treating individual days as statistically independent. For each replicate, recent-minus-historical differences in Tmax and eddy-Z500 were recalculated. The same year-clustered procedure was used to estimate uncertainty in the ATMI-conditioned heatwave-event probabilities shown in Fig. 4b. Two-sided 95% bootstrap intervals were defined by the 2.5th and 97.5th percentiles of the resulting bootstrap distributions. Correlations between 11-year running means are reported as descriptive measures of shared low-frequency evolution. The analysis remains observational, and serial dependence, event clustering, reference-pattern selection and covariance among slow forcings should be considered when interpreting uncertainty.

Data Availability

All data used in this study are publicly available. Daily maximum 2-m air temperature (Tmax), surface latent heat flux, 850-hPa geopotential and 500-hPa geopotential, converted to geopotential height, for 1950–2026 were obtained from ERA5[38]. Monthly sea surface temperature (SST) was obtained from NOAA ERSSTv5[39].

Code Availability

The code used to generate the analyses and figures in this study is available from authors upon reasonable request.

Acknowledgements

We thank the European Centre for Medium-Range Weather Forecasts (ECMWF) and the Copernicus Climate Change Service for providing the ERA5 reanalysis, and NOAA for providing the ERSSTv5 sea surface temperature dataset. We would like to acknowledge high-performance computing support from the Derecho system (doi:10.5065/qx9a-pg09) provided by the NSF National Center for Atmospheric Research (NCAR), sponsored by the National Science Foundation. This research was supported in part through research cyberinfrastructure resources and services provided by the Partnership for an Advanced Computing Environment (PACE) at the Georgia Institute of Technology, Atlanta, Georgia, USA. RRID:SCR_027619.

Contributions

H.W., F.Z. and G.W. conceived the study. H.W. performed the analyses. Y.W., H.-J.W. and F.Z. contributed to the investigation and interpretation of the results. H.-J.W. supervised the research. S.X. and W.L. contributed to data processing and analysis. H.W. and F.Z. wrote the original manuscript. All authors contributed to the discussion, revised the manuscript and approved the final version.

Ethics declarations

Competing interests

The authors declare no competing interests.

References

1. Stott PA, Stone DA, Allen MR. Human contribution to the European heatwave of 2003. *Nature* **432**, 610–614 (2004).

2. Schär C*, et al.* The role of increasing temperature variability in European summer heatwaves. *Nature* **427**, 332–336 (2004).

3. Della-Marta PM, Haylock MR, Luterbacher J, Wanner H. Doubled length of western European summer heat waves since 1880. *Journal of Geophysical Research: Atmospheres* **112**, D15103 (2007).

4. Fischer EM, Schär C. Consistent geographical patterns of changes in high-impact European heatwaves. *Nature Geoscience* **3**, 398–403 (2010).

5. Barriopedro D, Fischer EM, Luterbacher J, Trigo RM, García-Herrera R. The Hot Summer of 2010: Redrawing the Temperature Record Map of Europe. *Science* **332**, 220–224 (2011).

6. Christidis N, Jones GS, Stott PA. Dramatically increasing chance of extremely hot summers since the 2003 European heatwave. *Nature Climate Change* **5**, 46–50 (2015).

7. Perkins-Kirkpatrick SE, Lewis SC. Increasing trends in regional heatwaves. *Nature Communications* **11**, 3357 (2020).

8. Quilcaille Y*, et al.* Systematic attribution of heatwaves to the emissions of carbon majors. *Nature* **645**, 392–398 (2025).

9. Vautard R*, et al.* Heat extremes in Western Europe increasing faster than simulated due to atmospheric circulation trends. *Nature Communications* **14**, 6803 (2023).

10. Schumacher DL, Singh J, Hauser M, Fischer EM, Wild M, Seneviratne SI. Exacerbated summer European warming not captured by climate models neglecting long-term aerosol changes. *Communications Earth & Environment* **5**, 182 (2024).

11. Dong B, Sutton RT. Drivers and mechanisms contributing to excess warming in Europe during recent decades. *npj Climate and Atmospheric Science* **8**, 41 (2025).

12. Beobide-Arsuaga G, Suarez-Gutierrez L, Barkhordarian A, Olonscheck D, Baehr J. Increasing central and northern European summer heatwave intensity due to forced changes in internal variability. *Nature Communications* **16**, 9485 (2025).

13. Rousi E, Kornhuber K, Beobide-Arsuaga G, Luo F, Coumou D. Accelerated western European heatwave trends linked to more-persistent double jets over Eurasia. *Nature Communications* **13**, 3851 (2022).

14. Pfahl S, Wernli H. Quantifying the relevance of atmospheric blocking for co-located temperature extremes in the Northern Hemisphere on (sub-)daily time scales. *Geophysical Research Letters* **39**, L12807 (2012).

15. Horton DE, Johnson NC, Singh D, Swain DL, Rajaratnam B, Diffenbaugh NS. Contribution of changes in atmospheric circulation patterns to extreme temperature trends. *Nature* **522**, 465–469 (2015).

16. Kornhuber K*, et al.* Extreme weather events in early summer 2018 connected by a recurrent hemispheric wave-7 pattern. *Environmental Research Letters* **14**, 054002 (2019).

17. Woollings T*, et al.* Blocking and its Response to Climate Change. *Curr Clim Change Rep* **4**, 287–300 (2018).

18. Brunner L, Schaller N, Anstey J, Sillmann J, Steiner AK. Dependence of Present and Future European Temperature Extremes on the Location of Atmospheric Blocking. *Geophysical Research Letters* **45**, 6311–6320 (2018).

19. Wang L*, et al.* Gaps and ways forward in atmospheric blocking and extreme weather research. *Nature Communications* **17**, 2873 (2026).

20. Sutton RT, Hodson DLR. Atlantic Ocean Forcing of North American and European Summer Climate. *Science* **309**, 115–118 (2005).

21. Sutton RT, Dong B. Atlantic Ocean influence on a shift in European climate in the 1990s. *Nature Geoscience* **5**, 788–792 (2012).

22. Cassou C, Terray L, Phillips AS. Tropical Atlantic Influence on European Heat Waves. *Journal of Climate* **18**, 2805–2811 (2005).

23. Deser C, Alexander MA, Xie S-P, Phillips AS. Sea Surface Temperature Variability: Patterns and Mechanisms. *Annu Rev Mar Sci* **2**, 115–143 (2010).

24. O'Reilly CH, Woollings T, Zanna L, Weisheimer A. The Impact of Tropical Precipitation on Summertime Euro-Atlantic Circulation via a Circumglobal Wave Train. *Journal of Climate* **31**, 6481–6504 (2018).

25. Lim Y-K, Cullather RI, Nowicki SMJ, Kim K-M. Inter-relationship between subtropical Pacific sea surface temperature, Arctic sea ice concentration, and North Atlantic Oscillation in recent summers. *Scientific Reports* **9**, 3481 (2019).

26. Ossó A, Sutton R, Shaffrey L, Dong B. Observational evidence of European summer weather patterns predictable from spring. *Proceedings of the National Academy of Sciences* **115**, 59–63 (2018).

27. Beobide-Arsuaga G, Düsterhus A, Müller WA, Barnes EA, Baehr J. Spring Regional Sea Surface Temperatures as a Precursor of European Summer Heatwaves. *Geophysical Research Letters* **50**, e2022GL100727 (2023).

28. Krüger J, Kjellsson J, Kedzierski RP, Claus M. Connecting North Atlantic SST Variability to European Heat Events over the Past Decades. *TellusA* **75**, 358–374 (2023).

29. Qasmi S, Sanchez-Gomez E, Ruprich-Robert Y, Boé J, Cassou C. Modulation of the Occurrence of Heatwaves over the Euro-Mediterranean Region by the Intensity of the Atlantic Multidecadal Variability. *Journal of Climate* **34**, 1099–1114 (2021).

30. Czaja A, Frankignoul C. Observed Impact of Atlantic SST Anomalies on the North Atlantic Oscillation. *Journal of Climate* **15**, 606–623 (2002).

31. Qin M, Dai A, Hua W. Quantifying Contributions of Internal Variability and External Forcing to Atlantic Multidecadal Variability Since 1870. *Geophysical Research Letters* **47**, e2020GL089504 (2020).

32. Jézéquel A, Yiou P, Radanovics S. Role of circulation in European heatwaves using flow analogues. *Climate Dynamics* **50**, 1145–1159 (2018).

33. Zhang X*, et al.* Increased impact of heat domes on 2021-like heat extremes in North America under global warming. *Nature Communications* **14**, 1690 (2023).

34. Famooss Paolini L, Pascale S, Ruggieri P, Brattich E, Di Sabatino S. Drivers of summer extreme temperature trends in Europe: insight from three major heat waves using flow analogues. *Clim Dyn* **64**, 235 (2026).

35. Guo Y*, et al.* European compound flood-heat-flood events associated with Omega patterns cannot be easily reproduced by a fully coupled model. *Communications Earth & Environment* **6**, 491 (2025).

36. England MH*, et al.* Drivers of the extreme North Atlantic marine heatwave during 2023. *Nature* **642**, 636–643 (2025).

37. Guinaldo T, Cassou C, Sallée J-B, Liné A. Internal variability effect doped by climate change drove the 2023 marine heat extreme in the North Atlantic. *Communications Earth & Environment* **6**, 291 (2025).

38. Hersbach H*, et al.* The ERA5 global reanalysis. *Quarterly Journal of the Royal Meteorological Society* **146**, 1999–2049 (2020).

39. Huang B*, et al.* Extended Reconstructed Sea Surface Temperature, Version 5 (ERSSTv5): Upgrades, Validations, and Intercomparisons. *Journal of Climate* **30**, 8179–8205 (2017).

40. Perkins SE, Alexander LV. On the Measurement of Heat Waves. *Journal of Climate* **26**, 4500–4517 (2013).

41. Stefanon M, D'Andrea F, Drobinski P. Heatwave classification over Europe and the Mediterranean region. *Environmental Research Letters* **7**, 014023 (2012).

42. Wang H, Gao Y, Wang Y, Sheng L. Arctic sea ice modulation of summertime heatwaves over western North America in recent decades. *Environmental Research Letters* **17**, 074015 (2022).

43. Lhotka O, Kyselý J. Three-dimensional analysis reveals diverse heat wave types in Europe. *Communications Earth & Environment* **5**, 323 (2024).

44. Plavcová E, Lhotka O, Kyselý J. Heat Waves in Regional Climate Models: Three-Dimensional Insight and Links to Atmospheric Circulation Over Middle Europe. *Geophysical Research Letters* **52**, e2025GL115352 (2025).

45. North GR, Bell TL, Cahalan RF, Moeng FJ. Sampling Errors in the Estimation of Empirical Orthogonal Functions. *Monthly Weather Review* **110**, 699–706 (1982).

46. Luo B*, et al.* Increased Summer European Heatwaves in Recent Decades: Contributions From Greenhouse Gases-Induced Warming and Atlantic Multidecadal Oscillation-Like Variations. *Earth's Future* **11**, e2023EF003701 (2023).

47. Ghosh R, Müller WA, Eichhorn A, Baehr J, Bader J. Atmospheric pathway between Atlantic multidecadal variability and European summer temperature in the atmospheric general circulation model ECHAM6. *Climate Dynamics* **53**, 209–224 (2019).

48. Gu Q*, et al.* Wide range of possible trajectories of North Atlantic climate in a warming world. *Nature Communications* **15**, 4221 (2024).

49. Harrington LJ, Otto FEL, Cowan T, Hegerl GC. Circulation analogues and uncertainty in the time-evolution of extreme event probabilities: evidence from the 1947 Central European heatwave. *Climate Dynamics* **53**, 2229–2247 (2019).

50. Scott DW. *Multivariate Density Estimation: Theory, Practice, and Visualization*. John Wiley & Sons (1992).